J. Astrophys. Astr. (2021)42:90
https://doi.org/10.1007/s12036-021-09771-x

Photometric and kinematical analysis of Koposov 12 and Koposov 43 open clusters

W. H. ELSANHOURY[1,2]

[1]Physics Department, Faculty of Science and Arts, Northern Border University, Rafha Branch, Saudi Arabia.
[2]Astronomy Department, National Research Institute of Astronomy and Geophysics (NRIAG), 11421 Helwan, Cairo, Egypt.
*E-mail: elsanhoury@nbu.edu.sa; welsanhoury@gmail.com

MS received 5 March 2020; accepted 5 October 2020

Abstract. We present a photometric and kinematical analysis of two poorly studied open clusters, Koposov 12 (FSR 802) and Koposov 43 (FSR 848), by using cross-matched data from PPMXL and Gaia DR2 catalogs. We used astrometric parameters to identify 285 and 310 cluster members for Koposov 12 and Koposov 43, respectively. Using the extracted member candidates and isochrone fitting to near-infrared (J, H, and K_s) and Gaia DR2 bands (G, G_{BP}, and G_{RP}), and color-magnitude diagrams (CMDs), we have estimated ages: $\log(\text{age yr}^{-1}) = 9.00 \pm 0.20$ and 9.50 ± 0.20 and distances $d = 1850 \pm 43$ and 2500 ± 50 pc for Koposov 12 and Koposov 43, respectively, assuming solar metallicity ($Z = 0.019$). The estimated masses of the cluster derived using the initial mass function and synthetic (CMD) are 364 ± 19 and $352 \pm 19\, M_{\odot}$, respectively. We have also computed their velocity ellipsoid parameters based on (3×3) matrix elements (μ_{ij}).

Keywords. Open clusters: Koposov 12 (FSR 802) and Koposov 43 (FSR 848)—PPMXL and Gaia DR2—photometry: color-magnitude diagrams—stars: luminosity and mass functions—kinematics: dynamical evolution, velocity ellipsoid parameters.

1. Introduction

Open star clusters are interesting targets as they provide vital information on stellar structure, kinematics, and evolution of the Galactic disk (Yadav *et al.* 2011). The present paper is a part of our continuing series (Elsanhoury & Nouh 2019), the purpose of our research work is to determine the main astrophysical and kinematical properties of open clusters considering crossmatch between near-infrared region (NIR), J, H, and K_s, due to the positions and proper motions on the International Celestial Reference System (ICRS) (PPMXL catalog; Roeser *et al.* 2010) and Gaia photometric system, G, G_{BP}, and G_{RP} (Gaia DR2 catalog; Gaia Collaboration 2018).

Since a new interstellar extinction in the NIR, J, H, and K_s, provides an opportunity to profoundly burrow in the spiral arm regions where most of the open clusters are concentrated. The availability of huge NIR surveys allows researchers to perform an automated search to investigate new clusters (Yadav *et al.* 2011). Utilizing accessible information due to PPMXL by combining United States Naval Observatory (USNO-B1.0; Monet *et al.* 2003) all-sky catalog completeness down to $V = 21$ and the 2 μm all-sky survey catalogs (2MASS; Skrutskie *et al.* 2006) got to be confirmed by coordinating utilizing the later catalog such as a Global Astrometric Interferometer for Astrophysics Data Release 2 (Evans *et al.* 2018). Gaia data give recent reliable distances and kinematics to a large number of cluster members with higher accuracy. These recently available space parameters are very crucial and give clues to cluster disruption and the build-up of the field population (Fürnkranz *et al.* 2019). Recent publications making use of second Gaia data have provided membership lists for over 1000 clusters; however, many nearby objects listed in the literature have so far evaded detection (Cantat-Gaudin & Anders 2020).

The catalog of the second Gaia data release comes to a G-band magnitude of 21 (nine magnitudes fainter

Published online: 30 July 2021

than Tycho-Gaia Astrometric Solution (TGAS; Michalik *et al*. 2015). At its faint end, the Gaia DR2 astrometric precision is accurate with that of TGAS, whereas for stars brighter than ($G \lesssim 15$) the precision is about 10 times better than in TGAS, thus allowing to extend membership determinations to fainter and more distant objects (like our clusters under investigations). For more than 1.3 billion sources, the Gaia DR2 catalog presents five astrometric parameter solutions; central coordinates, proper motion in right ascension and declination, and parallaxes (α, δ, $\mu_\alpha \cos\delta$, μ_δ, and π); moreover, the magnitudes in the three passbands of the Gaia photometric system, G, $G_{\rm BP}$, and $G_{\rm RP}$, with precisions at the mmag level. Thus, leads to analyze the dynamical and kinematical evolutions.

Koposov *et al.* (2008) looked for Galactic star clusters in large multiband surveys to find new star clusters. Glushkova *et al.* (2010) recorded 168 newly open clusters, among which 26 are embedded ones. From this list, we have chosen two clusters: Koposov 12 (FSR 802) with a diameter of 9 arcmin; $(\alpha, \delta)_{2000} = (06^{\rm h}00^{\rm m}56^{\rm s}.20, 35^{\rm d}16^{\rm m}36^{\rm s}.00)$ with $(l, b) = (176^\circ.17014, 06^\circ.01963)$, and Koposov 43 (FSR 848) with a diameter of 8 arcmin; $(\alpha,\delta)_{2000} = (05^{\rm h}52^{\rm m}14^{\rm s}.60, 29^{\rm d}55^{\rm m}09^{\rm s}.00)$ with $(l,b) = (179^\circ.92431, 01^\circ.73987)$ (Koposov *et al.* 2008), in order to subject them to a photometric and kinematic investigation.

In this paper, we aim to understand the photometric and kinematic structures of these two open clusters. We have re-estimated their cluster parameters (reddening, distance modulus, and ages) concerned with J, H, K_s, G, $G_{\rm BP}$, and $G_{\rm RP}$ photometry using the membership selection based on the full astrometric solution (utilizing proper motions and magnitude uncertainties). On the other hand, our study of these two open clusters is the first one to estimate their kinematical and dynamical properties, into which we have computed their velocity ellipsoid parameters (VEPs) based on the spatial velocities estimation (U, V, and W), matrix elements (μ_{ij}), projected distances ($X_\odot$, $Y_\odot$, and $Z_\odot$), and solar elements ($S_\odot$, l_A, b_A, α_A, and δ_A).

This paper is organized in such a way that Section 2 describes the data used in this study to estimate the centers and surface density distribution. Section 3 deals with age, reddening, and distance. While Section 4 shows the luminosity and mass functions (LF and MF). Section 5 deals with the relaxation and internal motion processes of these open clusters due to the study of their dynamical and kinematical structures. Finally, the conclusion of this work is drawn in Section 6.

2. Data analysis

We have used the fundamental parameters of these two open clusters inferred by Koposov *et al.* (2008) and Sampedro *et al.* (2017), and the Milky Way Star Clusters project (Kharchenko *et al*. 2013), which is based on 2MASS (Skrutskie *et al.* 2006) photometry and PPMXL (Roeser *et al.* 2010) astrometry. The parameters are listed in Table 1.

For our purpose of analysis, we have cross-matched two sources of data. One is concerned with the second intermediate Gaia Data Release (Gaia DR2) for row data collected within the first 22 months of the nominal mission processed by the Gaia Data Processing and Analysis Consortium (DPAC). Gaia DR2 is setting a new major achievement for Gaia's mission in stellar, Galactic, and extra Galactic studies. It provides position, trigonometric parallax, radial velocity, and proper motions in both directions for more than 1 billion stars, as well as three broadband photometric magnitudes: G (330–1050 nm), the Blue Prism $G_{\rm BP}$ (330–680 nm), and Red Prism $G_{\rm RP}$ (630–1050 nm) for sources brighter than 21 mag (Weiler 2018).

The second source is devoted here with the PPMXL catalog (Roeser *et al.* 2010), which determines the mean positions and proper motions on the ICRS by combining USNO-B1.0 and 2MASS astrometry. PPMXL (Roeser *et al.* 2010) contains about 900 million objects, some 410 million with 2MASS photometry (Roeser *et al.* 2010). 2MASS had drawn photometric passband observations of the sky for millions of Galaxies and nearly half-billion stars (Carpenter 2001) simultaneously (NIR) regions; J (1.25 μm), H (1.65 μm), and K_s (2.17 μm) with sensitivity; J (5.8 mag), H (15.1 mag), and K_s (14.3 mag) bands at $S/N = 10$.

2.1 *Cluster center determination*

To start our calculations and to download complete row data, we utilized the Gaia DR2[1] source. Koposov 12 (FSR 802) and Koposov 43 (FSR 848) open clusters are located near the Galactic plane; $|b| < 6^\circ$, Koposov 12 (FSR 802) and $|b| < 2^\circ$, Koposov 43 (FSR 848) have diameters < 10 arcmin. To identify the

[1] https://vizier.u-strasbg.fr/viz-bin/VizieR?-source=I/345.

Table 1. Fundamental parameters of the two open clusters: Koposov 12 (FSR 802) and Koposov 43 (FSR 848).

Parameters	Koposov 12 (FSR 802)	Koposov 43 (FSR 848)	References
α	$06^h00^m55^s.99$	$05^h52^m15^s.00$	Sampedro *et al.* (2017)
	$06^h01^m02^s.64$	$05^h52^m17^s.40$	Kharchenko *et al.* (2013)
δ	$35^d16^m36^s.01$	$29^d55^m09^s.01$	Sampedro *et al.* (2017)
	$35^d16^m37^s.20$	$29^d53^m49^s.20$	Kharchenko *et al.* (2013)
l	176°.259	179°.901	Sampedro *et al.* (2017)
	176°.170	179°.924	Kharchenko *et al.* (2013)
b	05°.999	01°.744	Sampedro *et al.* (2017)
	06°.020	01°.740	Kharchenko *et al.* (2013)
Distance (pc)	2000	2800	Sampedro *et al.* (2017)
	1900	3000	Kharchenko *et al.* (2013)
$E(B-V)$ (mag)	0.510	0.380	Sampedro *et al.* (2017)
	0.450	0.650	Kharchenko *et al.* (2013)
log (age yr^{-1})	8.78	9.30	Sampedro *et al.* (2017)
	8.190	9.115	Kharchenko *et al.* (2013)
(*m*–*M*) (mag)	11.55 ± 0.03	12.21 ± 0.09	Koposov *et al.* (2008)
Diameter (arcmin)	9.00	8.00	Koposov *et al.* (2008)
V_r (km s^{-1})	13.6 ± 1.90	26.6 ± 0.90	Kharchenko *et al.* (2013)
μ_α (mas yr^{-1})	0.699 ± 0.009	-0.037 ± 0.021	Cantat-Gaudin *et al.* (2018)
μ_δ (mas yr^{-1})	-1.732 ± 0.011	-1.664 ± 0.014	Cantat-Gaudin *et al.* (2018)

extent of the cluster from the background stellar density, we use a radial density profile (RDP), where we performed star count over an extracted data within 10 arcmin. The data include angular distances (in arcmin) from the center, right ascension (in degrees), and declination (in degrees) with epoch 2015.0 about 3147 stars; Koposov 12 (FSR 802) and 4164 stars; Koposov 43 (FSR 848) open clusters are downloaded.

We performed binning along the right ascension (α) and declination (δ), with a bin size of 1.00 arcmin (Maciejewski & Niedzielski 2007; Maciejewski *et al.* 2009) by two opposite strips were cut along (α, δ). Figure 1 shows the resulting histogram, which was built along those (α, δ) and the two Gaussian curve fittings are applied to the profiles of star counts in right ascension (α) and declination (δ), respectively. Table 2 presents our estimated values of the new centers (i.e., maximum peaks) for both clusters, respectively, including the mean (average) (μ) with the standard errors taken to be ($\pm 1\sigma$) (i.e., standard deviation) of the Gaussian distribution function $f(x)$, i.e., $f(x) = (1/\sqrt{2\pi})\exp[-(x-\mu)^2/2\sigma^2]$. With such results, we may conclude that

- Our new results of right ascension (α) for Koposov 12 (FSR 802) bounded between Sampedro *et al.* (2017) and Kharchenko *et al.* (2013), where our estimation is greater by about $01^s.61$ that given by Sampedro *et al.* (2017) and smaller by about $05^s.04$ that given by Kharchenko *et al.* (2013). Also, our new estimation of declination (δ) is greater by about $19^s.19$ and $18^s.00$ for those both authors, respectively.
- On the other hand, the comparison may be accomplished with the other Koposov 43 (FSR 848) cluster into which our new estimation of right ascension (α) is smaller by about $00^s.12$ and $02^s.52$ with Sampedro *et al.* (2017) and Kharchenko *et al.* (2013), respectively. Other than that, our declination (δ) is smaller by about $04^s.21$ that given by Sampedro *et al.* (2017), and is greater by about $01^m15^s.60$ that given by Kharchenko *et al.* (2013).

2.2 *Radial density profile*

We downloaded a new worksheet data: 3173 stars, Koposov 12 (FSR 802) and 4162 stars, Koposov 43 (FSR 848), with our new center estimation shown in Table 2, we apply the King (1962) profile with annular bins; 0.90 arcmin (Koposov 12) and 1.00 arcmin (Koposov 43), to estimate their structural parameters, i.e., core radius ($r_{\rm core}$), central surface

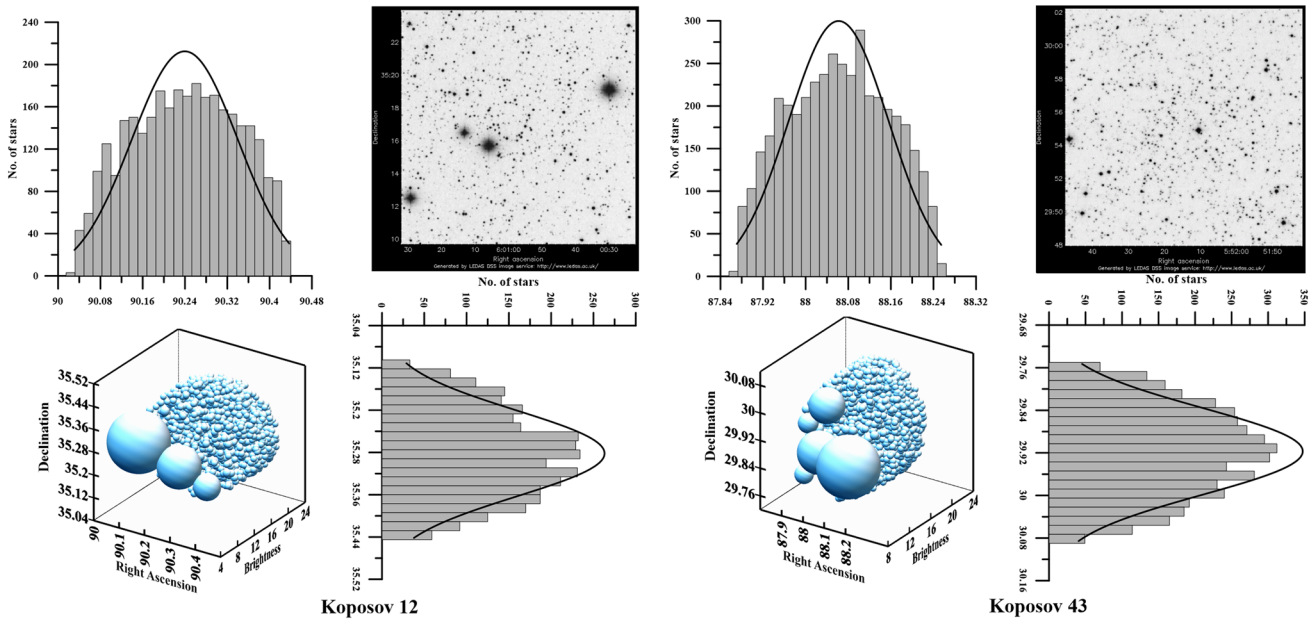

Figure 1. Images are taken from the LEicester Database and Archive Service Digitized Sky Survey (https://www.ledas.ac.uk/DSSimage) of Koposov 12 (FSR 802) and Koposov 43 (FSR 848) in the left: (upper right) and right: (upper right) panels, respectively. On the other hand, showing the 3D density of stars on the sky with Gaia DR2 of both clusters; left: (lower left) and right: (lower left) panels, respectively. The Gaussian fits (solid lines) provide the coordinates of highest density areas in (α) and (δ) for both clusters; diagonally of both panels, respectively.

Table 2. Our new center estimation for Koposov 12 (FSR 802) and Koposov 43 (FSR 848) open clusters.

Parameters	Koposov 12 (FSR 802) (3147 stars)	Koposov 43 (FSR 848) (4146 stars)
Max. peak (Ra.)	$90^{o}.240 \pm 0^{o}.101$	$88^{o}.062 \pm 0^{o}.095$
Max. peak (Dec.)	$35^{\circ}.282 \pm 0^{o}.082$	$29^{\circ}.918 \pm 0^{o}.082$
α	$06^{h}00^{m}57^{s}.60$	$05^{h}52^{m}\ 14^{s}.88$
δ	$35^{d}16^{m}55^{s}.20$	$29^{d}55^{m}04^{s}.80$
l	$176^{\circ}.148$	$179^{\circ}.922$
b	$6^{\circ}.007$	$1^{\circ}.741$

density (f_{o}), and background surface density (f_{bg}):

$$\rho(r) = f_{bg} + \frac{f_{o}}{1 + (r/r_{core})^{2}}. \quad (1)$$

Figure 2 shows the King model fit and its uncertainties (estimated using OriginPro package) for the density distribution of these two open clusters. In expansion, we will characterize the limiting radius (r_{lim}) (Tadross & Bendary 2014) as the radius at which the line represents the value of the background density that intersects the King model fitting curve. At this point, the background star density ($\rho_{b} = f_{bg} + 3\sigma_{bg}$), where ($\sigma_{bg}$) is the fluctuation (uncertainty) of the background surface density (f_{bg}). Mathematically, we have

$$r_{lim} = r_{core}\sqrt{\frac{f_{o}}{3\sigma_{bg}} - 1}. \quad (2)$$

In what takes after, we provided a microscopic investigation of our internal cluster structure estimation, counting r_{core}, f_{bg}, and f_{o}, where numerical values of these parameters are listed in Table 3. We may take note that our calculated core radius (r_{core}) is higher than by ~ 0.142 pc and smaller with 0.110 pc for both clusters, respectively, as compared with Kharchenko *et al.* (2013). Our limiting radius (r_{lim}) is smaller than by almost 0.014 and 1.294 pc for those clusters, respectively, as compared with Kharchenko *et al.* (2013) database.

On the other hand, for our case study, it is the first one ever to compute the density contrast parameter (δ_{c}) (i.e., $\delta_{c} = 1 + f_{o}/f_{bg}$) such as in Table 3. Interestingly, the density contrast parameter (δ_{c}) comes to high values ($7 \leq \delta_{c} \leq 23$) (Bonatto & Bica 2009) as expected from the compact star clusters.

The last row of Table 3 gives the concentration parameter (C) of these both clusters, which is concerned with the ratio between limiting and core radii (i.e., $C = r_{lim}/r_{core}$). Nilakshi *et al.* (2002) concluded that the angular size of the coronal region is almost

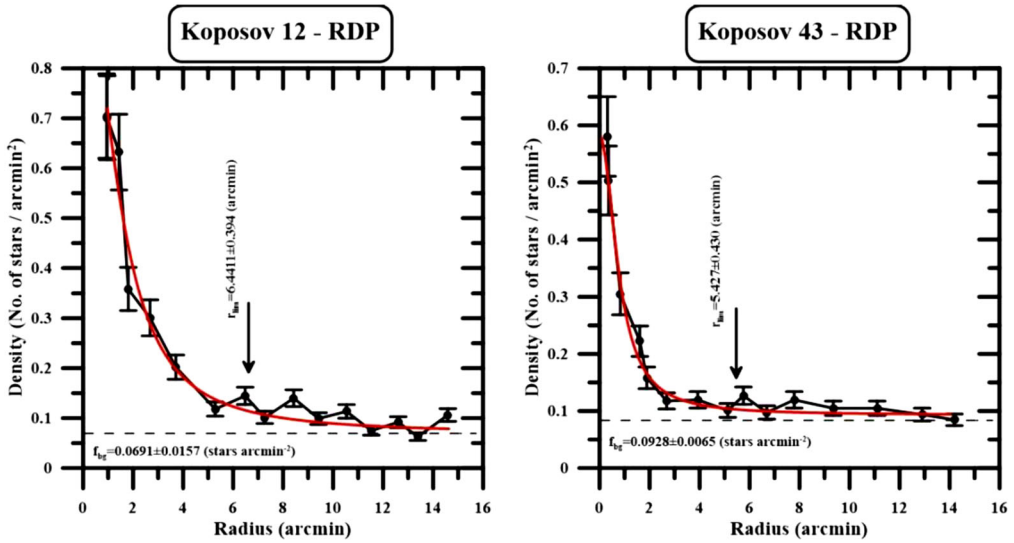

Figure 2. RDP of clusters: the left panel considered with Koposov 12 (FSR 802) and the right panel presents that for Koposov 43 (FSR 848) with error bars. The fitted solid lines were applied with King's model and the dashed lines represent the background field density (f_{bg}).

Table 3. Our results of the internal structure for Koposov 12 (FSR 802) and Koposov 43 (FSR 848) with other published ones.

Parameters	Koposov 12 (FSR 802)	Koposov 43 (FSR 848)	References
f_{bg} (stars arcmin^{-2})	0.069 ± 0.016	0.093 ± 0.006	Present study
f_o (stars arcmin^{-2})	0.921 ± 0.111	0.951 ± 0.028	Present study
r_{core} (pc)	0.805 ± 0.002	0.571 ± 0.003	Present study
	0.663	0.681	Kharchenko *et al.* (2013)
r_{lim} (pc)	3.466 ± 0.240	3.946 ± 0.213	Present study
	3.48	5.24	Kharchenko *et al.* (2013)
δ_c	14.324 ± 3.785	11.226 ± 3.351	Present study
C	4.305 ± 0.482	6.911 ± 0.380	Present study

($6r_{core}$). Whereas Maciejewski & Niedzielski (2007) detailed that (r_{lim}) extended between $2r_{core}$ and $7r_{core}$. Our concentration parameter (C) is in a good agreement with Maciejewski & Niedzielski (2007), which is about 4.305 ± 0.482 and 6.911 ± 0.380, respectively, for both clusters.

Now, our ultimate objective is to determine the space density (stars arcmin^{-3}). Consider for the stellar system (e.g., star clusters) with radius (R), the luminosity per unit volume at position r ($r < R$) shows that the surface brightness $I(R)$ and the luminosity density $j(r)$ are related by the formula (Binney & Termaine 2008)

$$I(R) = 2\int_R^\infty \mathrm{d}r \frac{rj(r)}{\sqrt{r^2 - R^2}}, \tag{3}$$

where

$$j(r) = -\frac{1}{\pi}\int_R^\infty \frac{\mathrm{d}R}{\sqrt{R^2 - r^2}}\frac{\mathrm{d}I}{\mathrm{d}R}. \tag{4}$$

The classical space density distribution (surface brightness per unit volume) in a specific direction of the Galactic plane of a given kind of association (e.g., star clusters) is usually determined by Blaauw & Schmidt (1965). Here the volume element (i.e., density) is determined by dividing the cluster into shells with a certain width depending on the number of stars in each radius interval (shell), then we divided the counts in each shell by the volume (zone) of this shell (van Rhijn 1965; Elsanhoury *et al.* 2011; Elsanhoury 2020).

To compute the star density (stars arcmin^{-3}) according to the Freedman & Diaconis (1981) rule, we can divide the above remarks of $n = 3173$ stars, Koposov 12 (FSR 802) and 4162 stars, Koposov 43 (FSR 848) into 16 and 17 groups, respectively, according to their radial distances (arcmin). Statistical steps in constructing a frequency distribution of these points under consideration are shown in Table 4, into which

- The number (k) of intervals can be determined with $k = (\text{max distance} - \text{min distance})/h$, where h is the bin width.
- The bin width (h) in Freedman & Diaconis (1981) is $h = (2 \times \text{IQR}/\sqrt[3]{n})$, where n is the sample size and IQR is the sample interquartile range.

Table 5 presents the intervals (classes) into which the first and second columns give the intervals (arcmin) and the center of the interval (arcmin), respectively, the third column presents the frequencies (counts), and the last column gives the density (stars arcmin^{-3}). Figure 3 shows our development volume density profile (VDP) (stars arcmin^{-3}) distribution of both clusters.

Table 4. Statistical parameters of Koposov 12 and Koposov 43 open clusters according to the Freedman & Diaconis (1981) rule.

Statistical parameters	Koposov 12 (FSR 802)	Koposov 43 (FSR 848)
n	3173	4162
Min. distance (arcmin)	0.1818	0.1365
Max. distance (arcmin)	9.9997	9.99959
IQR	4.707	4.834
h	0.641	0.601
k	16.00	17.00

3. Age, reddening, and distance

In this section, we need to determine many parameters of the cluster (reddening, distance modulus, and ages) due to a photometric analysis by constructing the color magnitude diagram (CMD) with a reduced field star contamination (i.e., established membership). Presently, Gaia DR2 catalog will be arranged to download worksheet row data with parallaxes greater than or equal to zero. Therefore, we have 558 stars (4.5 arcmin radius) of Koposov 12 (FSR 802) and 612 stars (4 arcmin radius) of Koposov 43 (FSR 848). Following the consideration devoted by Roeser *et al.* (2010),

Table 5. Frequency distribution of 3173 stars, Koposov 12 (FSR 802) and 4162 stars, Koposov 43 (FSR 848) open clusters under investigations.

Koposov 12 (FSR 802)				Koposov 43 (FSR 848)			
Intervals (arcmin)	Midpoint (arcmin)	Frequencies (counts)	Density (stars arcmin^{-3})	Intervals (arcmin)	Midpoint (arcmin)	Frequencies (counts)	Density (stars arcmin^{-3})
0.1818–0.8228	0.5023	23	9.9857	0.1365–0.7375	0.4370	31	18.6064
0.8228–1.4638	1.1433	66	6.1212	0.7375–1.3385	1.0380	68	8.1466
1.4638–2.1048	1.7843	93	3.5954	1.3385–1.9395	1.6390	114	5.5685
2.1048–2.7458	2.4253	114	2.3972	1.9395–2.5405	2.2400	157	4.1270
2.7458–3.3868	3.0663	146	1.9248	2.5405–3.1415	2.8410	183	2.9972
3.3868–4.0278	3.7073	156	1.4086	3.1415–3.7425	3.4420	194	2.1672
4.0278–4.6688	4.3483	175	1.1494	3.7425–4.3435	4.0430	215	1.7420
4.6688–5.3098	4.9893	214	1.0680	4.3435–4.9445	4.6440	220	1.3516
5.3098–5.9508	5.6303	221	0.8664	4.9445–5.5455	5.2450	258	1.2430
5.9508–6.5918	6.2713	259	0.8186	5.5455–6.1465	5.8460	259	1.0047
6.5918–7.2328	6.9123	270	0.7025	6.1465–6.7475	6.4470	330	1.0527
7.2328–7.8738	7.5533	288	0.6276	6.7475–7.3485	7.0480	327	0.8729
7.8738–8.5148	8.1943	337	0.6241	7.3485–7.9495	7.6490	353	0.8001
8.5148–9.1558	8.8353	303	0.4827	7.9495–8.5505	8.2500	399	0.7775
9.1558–9.7968	9.4763	385	0.5332	8.5505–9.1515	8.8510	388	0.6569
9.7968–10.4378	10.1173	123	0.1494	9.1515–9.7525	9.4520	459	0.6815
–	–	–	–	9.7525–10.3535	10.053	207	0.2717
$\Sigma = 3173$				$\Sigma = 4162$			

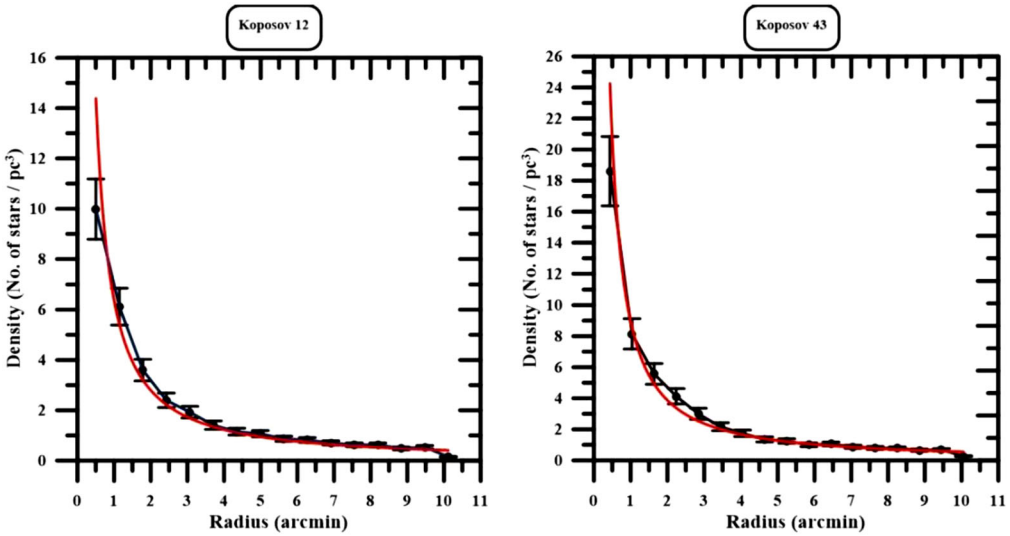

Figure 3. VDP (stars arcmin^{-3}) of Koposov 12 (FSR 802); left panel and Koposov 43 (FSR 848); right panel open clusters with error bars, respectively.

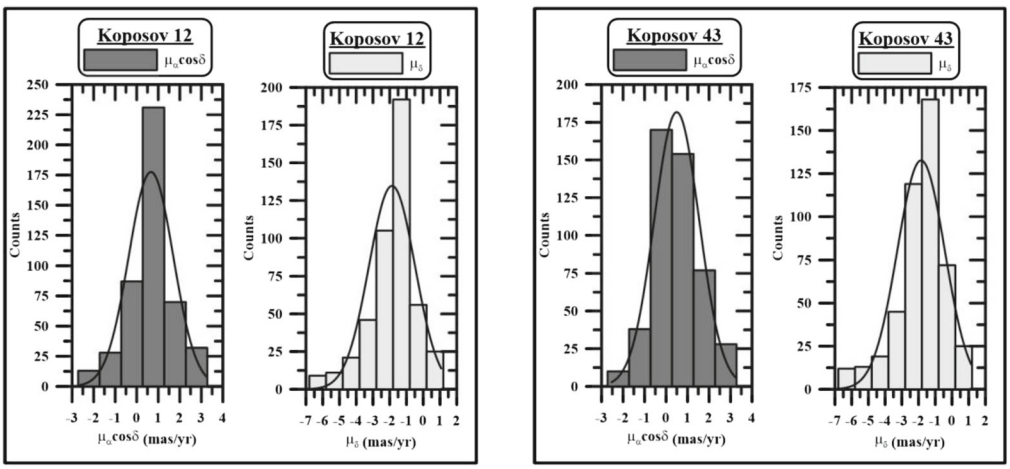

Figure 4. Proper motion VPD of proper motions in both directions with a Histogram of 1.00 (mas yr^{-1}) bins of Koposov 12 (FSR 802); left panel and Koposov 43 (FSR 848); right panel. The Gaussian fit to the central bins provides the mean in both directions. The data within the mean range ($\pm 1\sigma$) can be considered probable astrometric members (candidates).

into which (i) stars with proper motions uncertainties ≥ 4.0 (mas yr^{-1}) were rejected, (ii) stars with observational uncertainties ≥ 0.2 mag (Claria & Lapasset 1986). Therefore, the obtained results are 505 stars of Koposov 12 (FSR 802) and 534 stars of Koposov 43 (FSR 848).

Since proper motions play a vital role to separate field stars from the main sequence and to derive authentic fundamental parameters as well (Yadav *et al*. 2011; Sariya *et al*. 2018, 2019; Bisht *et al.* 2020a). Figure 4 shows a proper motion vector point diagram (VPD) on both sides with a distribution histogram of 1.00 (mas yr^{-1}) bins. The Gaussian function fit to the central bins provides the mean proper motion in both directions. Therefore (iii) all data within the range of mean ($\pm 1\sigma$) (where σ is the standard deviation of the mean) can be considered as highly probable astrometric members, i.e., 452 stars of Koposov 12 (FSR 802) and 438 stars of Koposov 43 (FSR 848), respectively.

Finally, we used these lists of members and interfere those with the PPMXL catalog (Roeser *et al.* 2010) via a cross-match to get a corresponding near a region of the clusters in *J*, *H*, and K_s pass-bands utilizing TOPCAT[2] (Taylor 2005) based on The Starlink Tables Infrastructure Library. It is powerful in our analysis for working with tabular data to evaluate a random number in the range of $0 \leq x < 1$, and offers many facilities for

[2]http://www.star.bris.ac.uk/∼mbt/topcat/.

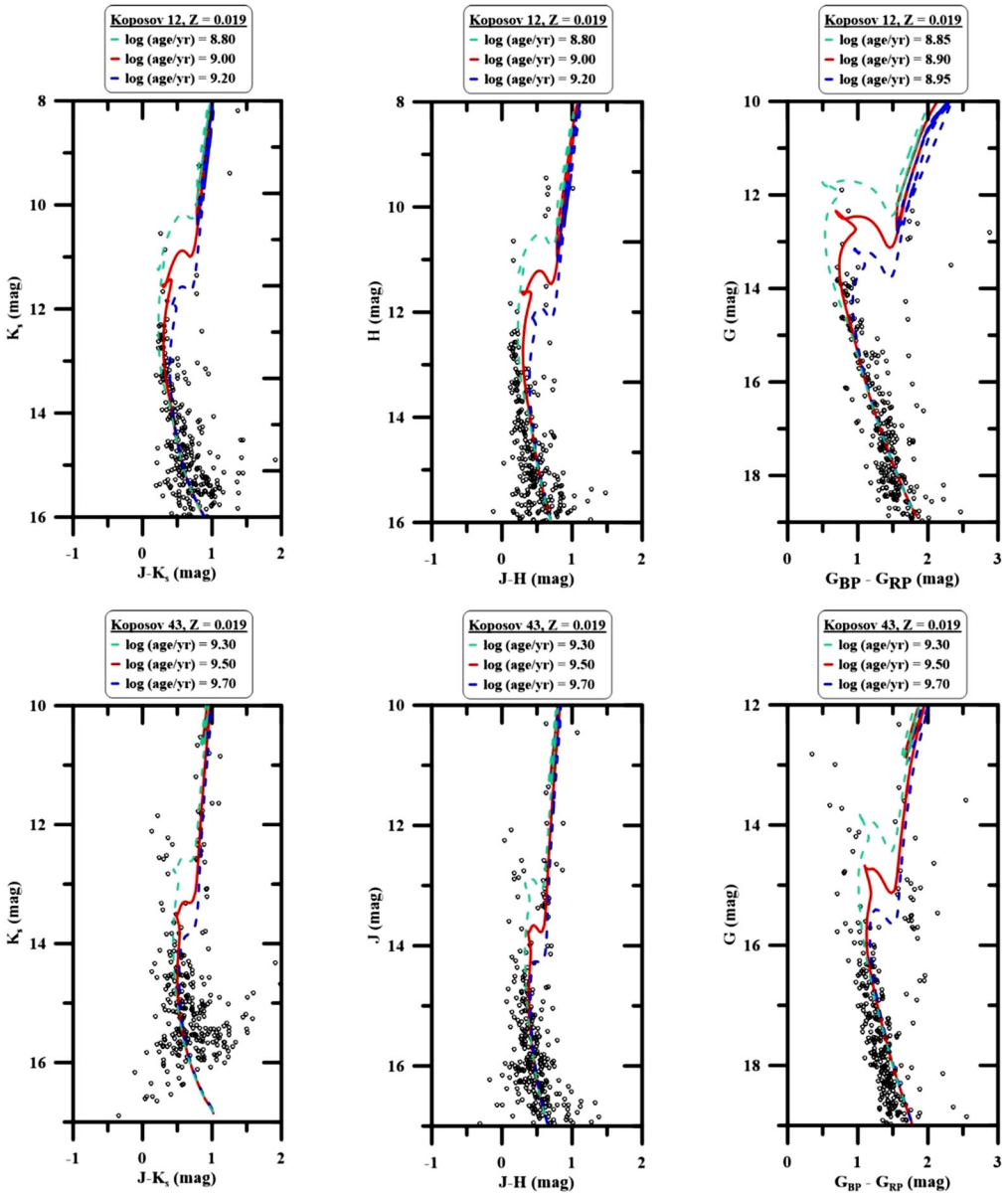

Figure 5. Padova color magnitude diagram (CMD) isochrones over [K_s *vs.* $(J - K_s)$, J *vs.* $(J - H)$, and G *vs.* $(G_{\rm BP} - G_{\rm RP})$] with Evans *et al.* (2018) for Koposov 12 (FSR 802): upper panel and Koposov 43 (FSR 848): lower panel.

manipulation of data such as astronomical catalogs. As a result of the above procedures, we have a high membership probability of $\geq 50\%$, i.e., 285 stars of Koposov 12 (FSR 802) and 310 stars of Koposov 43 (FSR 848), respectively.

The cluster parameters (reddening, distance modulus, and ages) were estimated with several isochrones of different ages with the theoretical Padova isochrones[3] (Marigo *et al.* 2017) for (J, H, K_s, G, $G_{\rm BP}$, and $G_{\rm RP}$) colors as in a case of Evans *et al.* (2018). The best fit should be obtained at the same distance modulus for both diagrams, and the reddening of the photometric system given by Fiorucci & Munari (2003).

Our fitted color-magnitude diagrams (CMDs) for (J–K, K_s), (J–H, J), and ($G_{\rm BP}$–$G_{\rm RP}$, G) mag are shown in Figure 5. All numerically astrophysical data appeared in Table 6 with comments.

Our estimation may be done with solar metallicity ($Z = 0.019$) (Froebrich *et al.* 2008) and are found in a region not heavily contaminated by field stars (Bonatto *et al.* 2004), we adopt $\log(\text{age yr}^{-1}) = 9.00 \pm 0.20$ for Koposov 12 (FSR 802), which is greater than those obtained (Sampedro *et al.* 2017; Kharchenko *et al.* 2013) by about $\log(\text{age yr}^{-1}) = 0.22$

[3] http://stev.oapd.inaf.it/cgi-bin/cmd.

Table 6. Comparison between our photometric parameters of Koposov 12 (FSR) and Koposov 43 (FSR 848) open clusters with different authors.

Parameters	Koposov 12 (FSR 802)	Koposov 43 (FSR 848)	References
log(age yr^{-1})	9.00 ± 0.20	9.50 ± 0.20	Present study
	8.78	9.30	Sampedro *et al.* (2017)
	8.190	9.115	Kharchenko *et al.* (2013)
	8.80	–	Yadav *et al.* (2011)
	9.00	9.3	Froebrich *et al.* (2008)
d (pc)	1850 ± 43	2500 ± 50	Present study
	2351.20	4787.50	Soubiran *et al.* (2018)
	2525.25	5555.56	Cantat-Gaudin *et al.* (2018)
	2000	2800	Sampedro *et al.* (2017)
	1900	3000	Kharchenko *et al.* (2013)
	2000 ± 200	–	Yadav *et al.* (2011)
	2050	2800	Froebrich *et al.* (2008)
$E(B-V)$	0.454 ± 0.05	0.482 ± 0.05	Present study
	0.51	0.38	Sampedro *et al.* (2017)
	0.45	0.65	Kharchenko *et al.* (2013)
	0.51 ± 0.05	–	Yadav *et al.* (2011)
$E(J-K_s)$	0.220 ± 0.06	0.233 ± 0.06	Present study
	0.216	0.312	Kharchenko *et al.* (2013)
$E(J-H)$	0.140 ± 0.08	0.149 ± 0.07	Present study
	0.144	0.208	Kharchenko *et al.* (2013)
$(m-M)$	11.60 ± 0.28	12.25 ± 0.28	Present study
	11.55 ± 0.03	12.21 ± 0.09	Koposov *et al.* (2008)

and 0.81, respectively; and $\log(\text{age yr}^{-1}) = 9.50 \pm 0.20$ for Koposov 43 (FSR 848), which is also greater than those obtained by same above authors by about $\log(\text{age yr}^{-1}) = 0.20$ and 0.385, respectively.

The reddening (color excess) of the clusters have been determined using the relations determined by Schlegel *et al.* (1998) and Schlafly & Finkbeiner (2011), where the coefficient ratios $A_J/A_V = 0.276$ and $A_H/A_V = 0.176$ are inferred using absorption ratios determined by Schlegel *et al.* (1998), whereas the ratio $A_K/A_V = 0.118$ was derived by Dutra *et al.* (2002). For our calculations with (J, H, K_s), we used the following results for the color excess of the photometric system by Fiorucci & Munari (2003); $E(J-H)/E(B-V) = 0.309 \pm 0.130$, $E(J-K_s)/E\ (B-V) = 0.485 \pm 0.150$, where $R_V = A_V/E(B-V) = 3.1$. By using these formulae for these two clusters under examination to rectify the effects of reddening on the color magnitude diagrams (CMDs) with extinction coefficients (A_V), i.e., $A_V = 1.407$ and 1.490, therefore the extinction coefficients for both clusters are $A = 0.276$ and 0.283, respectively. The line of sight extinction (A_G) and the reddening $E(G_{BP} - G_{RP})$ are estimated like in Hendy (2018) as $A_G/A_V = 0.859$ and $E(B-V) = 1.289E(G_{BP} - G_{RP})$. In this manner we have $A_G = 1.209$ and $E(G_{BP} - G_{RP}) = 0.352$ for Koposov 12 (FSR 802) and $A_G = 1.280$ and $E(G_{BP} - G_{RP}) = 0.374$ for Koposov 43 (FSR 848).

One of the most reasons for our CMDs is that it demonstrates the heliocentric distances $[d = 10^{([(m-M)-A+5]/5)}; \text{pc}]$ is of the order of about 1,850 ± 43 and 2,500 ± 50 pc, and the reddening $E(B-V)$ are almost 0.454 ± 0.05 and 0.482 ± 0.05 mag for Koposov 12 (FSR 802) and Koposov 43 (FSR 848), respectively.

4. Luminosity and mass functions

In this section, the luminosity function (LF) and mass function (MF) of the clusters have been estimated. Good results in the photometric parameters and position of the clusters have been obtained. Hence, we will induce their LF and describe the total number of stars in different absolute magnitudes and MF. Figure 6 presents LFs of Koposov 12 (FSR 802) and Koposov 43 (FSR 848) with absolute (M_{K_s})

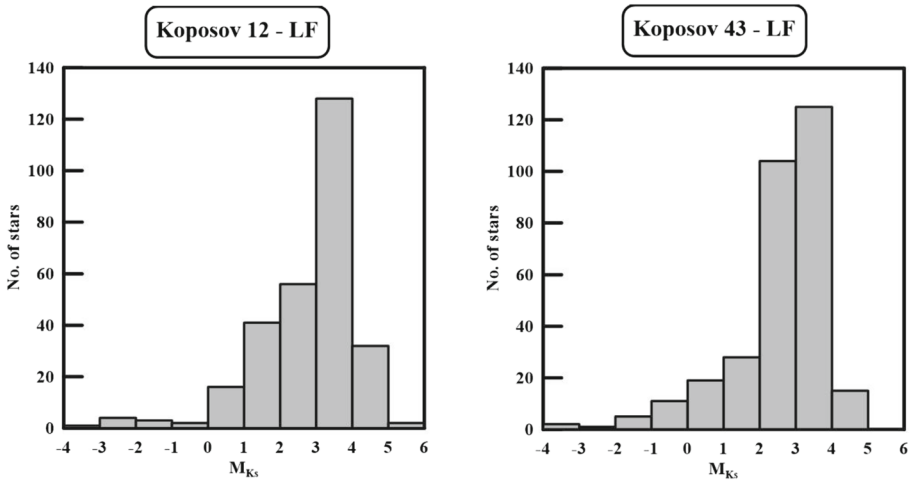

Figure 6. Left panel presents the LF of Koposov 12 (FSR 802), while the right panel shows that for the Koposov 43 (FSR 848) open cluster.

magnitude in the range $-3.415 < M_{K_s} < 5.658$ and $-3.234 < M_{K_s} < 4.982$, respectively. The total luminosities have computed for both clusters with values of 2.84 ± 1.37 and 2.57 ± 1.33 mag, respectively. Mass segregation massive stars are concentrated toward the cluster core than fainter ones and this phenomenon has been reported recently for many open clusters (Piatti 2016; Zeidler *et al.* 2017; Dib *et al.* 2018; Rangwal *et al.* 2019; Bisht *et al.* 2020b; Joshi *et al.* 2020).

To compute the MF of these open clusters, we have characterized the initial MF (IMF) with power law as follows:

$$\frac{\mathrm{d}N}{\mathrm{d}M} = M^{-\Gamma}, \tag{5}$$

where $(\mathrm{d}N/\mathrm{d}M)$ is the number of stars on the mass interval $(M: M + \mathrm{d}M)$ and (Γ) is a dimensionless exponent. From Salpeter (1955), the IMF for massive stars $(>1M_{\odot})$ has been considered and well built-up (i.e., $\Gamma = 2.35$).

According to the well-known MLR and accounting the absolute magnitudes (M_{K_s}) and masses $(M/M_{\odot})$ of the adopted isochrones (Evans *et al.* 2018), we can infer the MLR of each cluster (Elsanhoury & Nouh 2019). This relationship is polynomial functions of the second order for two ranges of luminosities, as shown in Figure 7. Therefore,

- For Koposovs 12 (FSR 802):

$$\left[\frac{M}{M_{\odot}}\right]_{\text{Koposov 12}} = 2.042 - 0.162M_{K_s} - 0.032M_{K_s}^2. \tag{6}$$

- For Koposovs 43 (FSR 848):

$$\left[\frac{M}{M_{\odot}}\right]_{\text{Koposov 43}} = 1.476 - 0.055M_{K_s} - 0.024M_{K_s}^2. \tag{7}$$

Then, the total masses are 364 ± 19 $M_{\odot}$ and 352 ± 19 $M_{\odot}$ for Koposov 12 and Koposov 43, respectively.

Figure 8 presents the MFs of these open clusters with error bars, showing their fitted line with slopes -2.62 ± 0.56 (Koposov 12) and -2.22 ± 0.90 (Koposov 43), which are in good agreement with Salpeter's value (1955).

5. Dynamical and kinematical structures

Now, we are going to consider the dynamical and kinematical processes involved in these two open clusters, the results obtained are shown in Table 7 with comments.

It is known that in the Galactic disk, the effect on the gravitational massive body (e.g., star cluster) is given by Röser & Elena (2019) equation, i.e.,

$$x_L = \left[\frac{GM_C}{4A(A-B)}\right]^{1/3} = \left[\frac{GM_C}{4\Omega_o^2 - \kappa^2}\right]^{1/3}, \tag{8}$$

where x_L is the gap of the Lagrangian points within the center, M_C is the sum of the collective mass (with Equations (6) and (7)) toward the gap from the center, which is mentioned to be the tidal radius (r_t) of the cluster (i.e., $x_L \approx r_t$) into which the star undergoes equal forces due to the gravitational pull toward the cluster and in the opposite

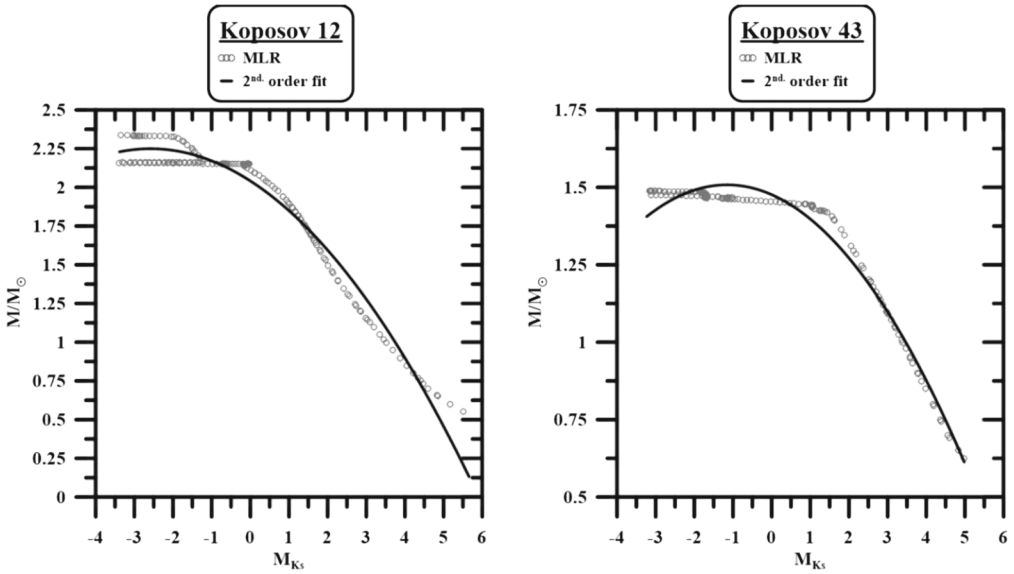

Figure 7. MLR between absolute magnitude (M_{K_s}) and masses ($M/M_\odot$) with solar metallicity ($Z = 0.019$) (gray circles) from isochrones (Evans *et al.* 2018) and its fitted lines (black solid) for Koposov 12 (FSR 802, left panel) and Koposov 43 (FSR 848, right panel).

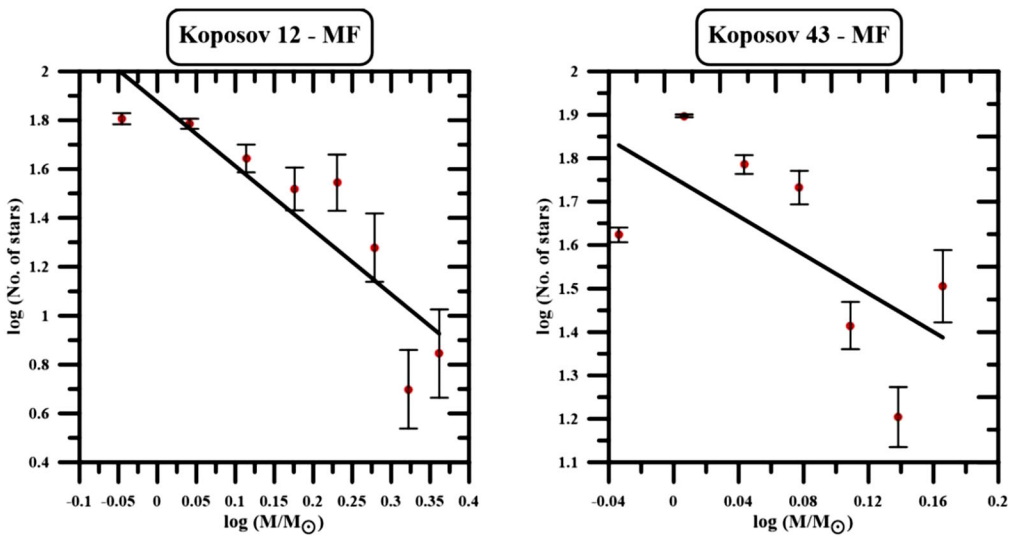

Figure 8. The MFs of both Koposov 12 (FSR 802, left panel) and Koposov 43 (FSR 848, right panel) with their fitted lines.

direction (i.e., the Galactic center), ($\Omega_o = A - B$) the angular velocity and ($\kappa = \sqrt{-4B(A-B)}$) the epicyclic frequency at the position of the Sun (both in $\mathrm{km\,s^{-1}\,kpc^{-1}}$) (Röser *et al.* 2011), (A) and (B) are Oort's constants: 15.3 ± 0.4 and $-11.9 \pm 0.4\,\mathrm{km\,s^{-1}\,kpc^{-1}}$ with Bovy (2017) and also equals to 15.6 ± 1.6 and $-13.9 \pm 1.8\,\mathrm{km\,s^{-1}\,kpc^{-1}}$ by Nouh & Elsanhoury (2020), and $G = 4.30 \times 10^{-6}\,\mathrm{kpc}\,M_\odot^{-1}\,(\mathrm{km\,s^{-1}})^2$ is the gravitational constant. In such a way, our obtained $r_t \approx 9.80 \pm 3.13$ pc as a function of our total estimated masses (M_C) for Koposov 12 (FSR 802) and 9.70 ± 3.11 pc for Koposov 43 (FSR) clusters.

Due to forces of contraction and/or destruction, open clusters come to the Maxwellian stability equilibrium with a time characterized as a relaxation time (T_{relax}), into which the cluster will lose all traces of its initial dynamic condition (Yadav *et al.* 2011; Bisht *et al.* 2019). T_{relax} depends on dynamical crossing time (T_{cross}) and the number (N) of member stars (Lada & Lada 2003). During relaxation time (T_{relax}), low mass stars possess the largest random velocity,

Table 7. Our dynamical and kinematical parameters of Koposov 12 (FSR 802) and Koposov 43 (FSR 848) open clusters.

Parameters	Koposov 12 (FSR 802)	Koposov 43 (FSR 848)	References
No. of members (N)	285	310	Present study
$\mu_\alpha \cos\delta$ (mas yr^{-1})	0.632 ± 0.006	0.517 ± 0.057	Present study
μ_δ (mas yr^{-1})	−1.945 ± 0.006	−1.810 ± 0.057	Present study
Luminosity (mag)	2.84 ± 1.37	2.57 ± 1.33	Present study
Γ	2.62 ± 0.56	2.22 ± 0.90	Present study
Total mass M_c ($M_\odot$)	364 ± 19	352 ± 19	Present study
Average mass ($M_\odot$)	1.276	1.138	Present study
r_t (pc)	9.80 ± 3.13	9.70 ± 3.11	Present study
T_{cross} (Myr)	10.316 ± 3.22	12.750 ± 3.57	Present study
T_{relax} (Myr)	65.017 ± 8.06	86.125 ± 9.28	Present study
τ_{ev} (Myr)	6501 ± 80.67	8613 ± 92.81	Present study
τ	15.38 ± 3.92	36.72 ± 6.06	Present study
V_{esc} (km s^{-1})	311 ± 5.67	332 ± 5.48	Present study
($\overline{V}_x$, $\overline{V}_y$, $\overline{V}_z$) (km s^{-1})	−15.62 ± 3.95, 32.50 ± 5.70, −22.50 ± 4.74	−31.17 ± 5.58, 55.68 ± 7.46, −41.56 ± 6.45	Present study
($\overline{U}$, $\overline{V}$, $\overline{W}$) (km s^{-1})	−16.60 ± 4.07, −39.03 ± 6.25, −2.80 ± 0.60	−26.74 ± 5.17, −71.27 ± 8.44, −2.27 ± 0.66	Present study
	−21.81 ± 1.44, −19.24 ± 0.29, −0.46 ± 0.19	2.22 ± 1.88, −32.09 ± 1.73, −20.01 ± 1.14	Soubiran *et al.* (2018)
(λ_1, λ_2, λ_3) (km s^{-1})	13841.10, 827.71, 134.46	236661.82, 8411.11, 608.45	Present study
(σ_1, σ_2, σ_3) (km s^{-1})	117.65, 28.77, 11.60	486.48, 91.71, 24.67	Present study
σ_V (km s^{-1})	122 ± 9.00	496 ± 4.50	Present study
(l_1, m_1, n_1)°	0.088, 0.983, −0.158	0.002, −0.921, 0.389	Present study
(l_2, m_2, n_2)°	−0.313, −0.123, −0.942	−0.129, −0.386, −0.913	Present study
(l_3, m_3, n_3)°	0.946, −0.133, −0.297	0.992, −0.048, −0.120	Present study
(x_c, y_c, z_c) (pc)	−17.074, 3792.7, 2683.33	334.563, 10042.5, 5787.05	Present study
B_j, j = 1, 2, 3	−9°.100, −70°.359, −17°.253	22°.902, −65°.977, −6°.865	Present study
L_j, j = 1, 2, 3	−84°.865, 158°.471, −172°.014	89°.589, 108°.446, −177°.226	Present study
$X_\odot$ (kpc)	−1.836 ± 0.043	−2.499 ± 0.050	Present study
	−2.333	−4.7852	Cantat-Gaudin *et al.* (2018)
$Y_\odot$ (kpc)	0.124 ± 0.001	0.004 ± 0.0002	Present study
	0.1568 ± 0.002	0.006 ± 0.0003	Soubiran *et al.* (2018)
	0.1568	0.0064	Cantat-Gaudin *et al.* (2018)
$Z_\odot$ (kpc)	0.194 ± 0.0014	0.076 ± 0.009	Present study
	0.2603 ± 0.0029	0.1599 ± 0.0077	Soubiran *et al.* (2018)
	0.2463	0.1459	Cantat-Gaudin *et al.* (2018)
R_{gc} (kpc)	9.347 ± 0.097	10.00 ± 0.100	Present study
	10.6742	13.1252	Cantat-Gaudin *et al.* (2018)
	10.50	–	Yadav *et al.* (2011)
	10.00	10.90	Froebrich *et al.* (2008)
$S_\odot$ (km s^{-1})	42.50	76.15	Present study
$(l_A, \alpha_A)^\circ_{\text{w.s.v.c.}}$	−66.96, 3.77	−69.44, 1.71	Present study
$(b_A, \delta_A)^\circ_{\text{w.r.v.c.}}$	−64.33, 31.96	−60.76, 33.08	Present study

possessing a bigger volume than the high mass does (Mathieu & Latham 1986). Mathematically, relaxation time (T_{relax}) has the form:

$$T_{relax} = \frac{N}{8 \ln N} T_{cross}. \quad (9)$$

where $T_{cross} = D/\sigma_V$ is the dynamical crossing time; namely defined as the time needed (independent of the size and shape of the orbit) for the cluster to cross the Galaxy once (Binney & Merrifield 1998). Typically, crossing time (T_{cross}) in open clusters is $\sim 10^6$ years

(Lada & Lada 2003) and D is the cluster diameter (Maciejewski & Niedzielski 2007) with expression corresponding to Lada & Lada (2003) as ($D \simeq 2r_{\rm lim}$). All numerical values of crossing time ($T_{\rm cross}$) and relaxation time ($T_{\rm relax}$) are drawn here with those in Table 7.

For enough cluster members, the time needed to eject all its members from internal stellar encounters defined as the evaporation time ($\tau_{\rm ev}$) (Adams & Myers 2001) to be $>10^8$ years; ($\tau_{\rm ev}$) for a stellar system in virial equilibrium is of the order 10^2 ($T_{\rm relax}$). The escaping velocity of stars from the cluster is defined as $V_{\rm esc} = R_{\rm gc}\sqrt{2GM_C/3r_t^3}$) (Fich & Tremaine 1991; Fukushige & Heggie 2000) and must be less than the dispersion velocity (σ_V) (Lada & Lada 2003). Thus, a bound group will emerge only if the star-formation efficiency (characterizes most cluster-forming dense cores) is >50% (Wilking & Lada 1983).

Finally, we can describe the dynamical state of these clusters by computing their dynamical evolution parameter ($\tau = {\rm age}/T_{\rm relax}$). If the cluster age was founded greater than its relaxation time, i.e., $\tau \gg 1$ then the cluster was dynamically relaxed and vice versa.

Now, we focused on some kinematics and VEPs for our objects with member (N) stars due to the computational algorithm presented (Elsanhoury 2015; Elsanhoury *et al*. 2015, 2016, 2018; Bisht *et al*. 2020a; Postnikova *et al*. 2020) by considering members coordinated with (α, δ) located at a distance d_i (pc), proper motions (mas yr^{-1}) in both directions and radial velocities V_r (km s^{-1}), which are listed in Table 1. Therefore, and according to the well-known basic equations that governs the positions (x, y, z; pc) from the Sun along with the equatorial system and distance d (pc) of the star members (Mihalas & Binney 1981), i.e.,

$$x = d\cos\delta\cos\alpha, \tag{10}$$

$$y = d\cos\delta\sin\alpha, \tag{11}$$

$$z = d\sin\delta. \tag{12}$$

In this method, differentiating Equations (10)–(12) with respect to time, we obtain the velocity components (V_x, V_y, V_z; km s^{-1}) along x, y, and z axes in the coordinate system with respect to the Sun (Smart 1968), i.e.,

$$V_x = -4.74d_i\mu_\alpha\cos\delta\sin\alpha - 4.74d_i\mu_\delta\sin\delta\cos\alpha + V_r\cos\delta\cos\alpha, \tag{13}$$

$$V_y = +4.74d_i\mu_\alpha\cos\delta\cos\alpha - 4.74d_i\mu_\delta\sin\delta\sin\alpha + V_r\cos\delta\sin\alpha, \tag{14}$$

$$V_z = +4.74d_i\mu_\delta\cos\delta + V_r\sin\delta. \tag{15}$$

To obtain the components of space velocities (U, V, W) along with Galactic coordinates as a function of space stellar velocities (V_x, V_y, V_z) whose definite to the Sun were derived with Liu *et al.* (2011); i.e., from the equatorial to the Galactic coordinates, based on NIR by 2MASS (Skrutskie *et al.* 2006) and radio observation data, i.e.,

$$U = -0.0518807421V_x - 0.8722226427V_y - 0.4863497200V_z, \tag{16}$$

$$V = +0.4846922369V_x - 0.4477920852V_y + 0.7513692061V_z, \tag{17}$$

$$W = -0.8731447899V_x - 0.1967483417V_y + 0.4459913295V_z. \tag{18}$$

In this section, we will give a brief description of the algorithm mentioned above. Let (ξ) and its zero points focuses coincide with the center of the distribution and let (l, m, and n) be the direction cosines of the axis with respect to the shifted one, then the coordinates (Q_i) of the point (i) with respect to the ξ-axis are given by

$$Q_i = l(U_i - \overline{U}) + m(V_i - \overline{V}) + n(W_i - \overline{W}), \tag{19}$$

where ($\overline{U}$, $\overline{V}$, and $\overline{W}$) are the mean velocities and considering (σ^2) maybe a generalization of the mean square deviation, i.e.,

$$\sigma^2 = \frac{1}{N}\sum_{i=1}^{N} Q_i^2. \tag{20}$$

Using the mean velocities ($\overline{U}$, $\overline{V}$, and $\overline{W}$), and Equations (19) and (20), one deduces that

$$\sigma^2 = \underline{x}^{\rm T} B \underline{x}, \tag{21}$$

where ($\underline{x}$) is the (3×3) direction cosines vector and B is the (3×3) symmetric matrix with elements (μ_{ij}):

$$\mu_{11} = \frac{1}{N}\sum_{i=1}^{N} U_i^2 - (\overline{U})^2, \mu_{12} = \frac{1}{N}\sum_{i=1}^{N} U_iV_i - \overline{UV},$$
$$\mu_{13} = \frac{1}{N}\sum_{i=1}^{N} U_iW_i - \overline{UW}, \mu_{22} = \frac{1}{N}\sum_{i=1}^{N} V_i^2 - (\overline{V})^2,$$
$$\mu_{23} = \frac{1}{N}\sum_{i=1}^{N} V_iW_i - \overline{VW}, \mu_{33} = \frac{1}{N}\sum_{i=1}^{N} W_i^2 - (\overline{W})^2. \tag{22}$$

Now, the necessary condition for an extremum is as follows:

$$(B - \lambda I)\underline{x} = 0. \tag{23}$$

These are three homogeneous equations in three unknowns that have a nontrivial solution if and only if

$$D(\lambda) = |B - \lambda I| = 0. \tag{24}$$

The above equation is the characteristic equation for the matrix B, where λ is the eigenvalue, $\underline{x}$ and B could be written as

$$\overline{x} = \begin{bmatrix} l \\ m \\ n \end{bmatrix} \quad \text{and} \quad B = \begin{vmatrix} \mu_{11} & \mu_{12} & \mu_{13} \\ \mu_{21} & \mu_{22} & \mu_{23} \\ \mu_{31} & \mu_{32} & \mu_{33} \end{vmatrix}.$$

Then, the required roots (i.e., eigenvalues) are

$$\begin{aligned} \lambda_1 &= 2\rho^{\frac{1}{3}} \cos\frac{\phi}{3} - \frac{k_1}{3}, \\ \lambda_2 &= -\rho^{\frac{1}{3}} \left\{ \cos\frac{\phi}{3} + \sqrt{3}\sin\frac{\phi}{3} \right\} - \frac{k_1}{3}, \\ \lambda_3 &= -\rho^{\frac{1}{3}} \left\{ \cos\frac{\phi}{3} - \sqrt{3}\sin\frac{\phi}{3} \right\} - \frac{k_1}{3}, \end{aligned} \tag{25}$$

where

$$\begin{aligned} k_1 &= -(\mu_{11} + \mu_{22} + \mu_{33}), \\ k_2 &= \mu_{11}\mu_{22} + \mu_{11}\mu_{33} + \mu_{22}\mu_{33} - \left(\mu_{12}^2 + \mu_{13}^2 + \mu_{23}^2\right), \\ k_3 &= \mu_{12}^2\mu_{33} + \mu_{13}^2\mu_{22} + \mu_{23}^2\mu_{11} - \mu_{11}\mu_{22}\mu_{33} \\ &\quad - 2\mu_{12}\mu_{13}\mu_{23}. \end{aligned} \tag{26}$$

$$q = \frac{1}{3}k_2 - \frac{1}{9}k_1^2; \quad r = \frac{1}{6}(k_1 k_2 - 3k_3) - \frac{1}{27}k_1^3, \tag{27}$$

$$\rho = \sqrt{-q^3}, \tag{28}$$

$$x = \rho^2 - r^2, \tag{29}$$

and

$$\phi = \tan^{-1}\left(\frac{\sqrt{x}}{r}\right). \tag{30}$$

Depending on the matrix that controls the eigenvalue problem (Equation 24) for the velocity ellipsoid, we built up analytical expressions of some parameters in terms of the (3×3) matrix elements (μ_{ij}). Table 7 shows all those numerical results.

- *The direction cosines parameters:* The direction cosines (l_j, m_j, and n_j; $\forall j$ = 1, 2, 3) for the eigenvalue problem (λ), matrix elements (μ_{ij}), and dispersion velocities (σ_j) (i.e., $\sigma_j = \sqrt{\lambda_j}$; $\forall j$ = 1, 2, 3) along three axes (Elsanhoury *et al.* 2015) are mathematically given by the following:

$$l_j = \left[\mu_{22}\mu_{33} - \sigma_i^2\left(\mu_{22} + \mu_{33} - \sigma_i^2\right) - \mu_{23}^2\right]/D_j, \tag{31}$$

$$m_j = \left[\mu_{23}\mu_{13} - \mu_{12}\mu_{33} + \sigma_j^2\mu_{12}\right]/D_j, \tag{32}$$

$$n_j = \left[\mu_{12}\mu_{23} - \mu_{13}\mu_{22} + \sigma_j^2\mu_{13}\right]/D_j, \tag{33}$$

where ($l_j^2 + m_j^2 + n_j^2 = 1$) as the initial test for our code with our sample and

$$\begin{aligned} D_j^2 &= \left(\mu_{22}\mu_{33} - \mu_{23}^2\right)^2 + \left(\mu_{23}\mu_{13} - \mu_{12}\mu_{33}\right)^2 \\ &\quad + \left(\mu_{12}\mu_{23} - \mu_{13}\mu_{22}\right)^2 \\ &\quad + 2[(\mu_{22} + \mu_{33})\left(\mu_{23}^2 - \mu_{22}\mu_{33}\right) \\ &\quad + \mu_{12}(\mu_{23}\mu_{13} - \mu_{12}\mu_{33}) \\ &\quad + \mu_{13}(\mu_{12}\mu_{23} - \mu_{13}\mu_{22})]\sigma_j^2 \\ &\quad + \left(\mu_{33}^2 + 4\mu_{22}\mu_{33} + \mu_{22}^2 - 2\mu_{23}^2 + \mu_{12}^2 + \mu_{13}^2\right)\sigma_j^4 \\ &\quad - 2(\mu_{22} + \mu_{33})\sigma_j^6 + \sigma_j^8. \end{aligned}$$

- *The Galactic longitude and latitude parameters:* Let (L_j) and (B_j), ($\forall j$ = 1, 2, 3) be the Galactic longitude and latitude of the directions, respectively, which correspond to the extreme values of the dispersion, then

$$L_j = \tan^{-1}\left(\frac{-m_j}{l_j}\right), \tag{34}$$

$$B_j = \sin^{-1}\left(n_j\right). \tag{35}$$

- *The center of the cluster:* The center of the cluster (x_c, y_c, z_c) can be derived by the simple method of finding the equatorial coordinates of the center of mass for the number (N_i) of discrete objects, i.e.,

$$x_c = \left[\sum_{i=1}^{N} d_i \cos\alpha_i \cos\delta_i\right] \Big/ N, \tag{36}$$

$$y_c = \left[\sum_{i=1}^{N} d_i \sin\alpha_i \cos\delta_i\right] \Big/ N, \tag{37}$$

$$z_c = \left[\sum_{i=1}^{N} d_i \sin\delta_i\right] \Big/ N. \tag{38}$$

- *Projected distances:* Considering our estimated distances d (pc) with over markers, consequently, we infer to include those distances to the Galactic

center (R_{gc}) (Mihalas & Binney 1981) like a function of the Sun's distance from the Galactic center (i.e., $R_o = 8.20 \pm 0.10$ kpc) as mentioned recently (Bland-Hawthorn *et al.* 2019); i.e., $R_{gc}^2 = R_o^2 + d^2 - 2R_o d\cos l$, in such a way the anticipated (projected) distances toward the Galactic plane ($X_\odot, Y_\odot$) and the distance from the Galactic plane ($Z_\odot$) (Tadross 2011) maybe computed as follows:

$$X_\odot = d\cos b\cos l, \tag{39}$$

$$Y_\odot = d\cos b\sin l, \tag{40}$$

$$Z_\odot = d\sin b. \tag{41}$$

- *Solar elements:* Consider a group with spatial velocities ($\overline{U}$, $\overline{V}$, and $\overline{W}$). The components of Sun's velocities are ($U_\odot$, $V_\odot$, and $W_\odot$) are given as ($U_\odot = -\overline{U}$), ($V_\odot = -\overline{V}$), and ($W_\odot = -\overline{W}$). Therefore, we have the solar elements with spatial velocities considered w.s.v.c. like

$$S_\odot = \sqrt{\overline{U}^2 + \overline{V}^2 + \overline{W}^2}, \tag{42}$$

$$l_A = \tan^{-1}\left(\frac{-\overline{V}}{\overline{U}}\right), \tag{43}$$

$$b_A = \sin^{-1}\left(\frac{-\overline{W}}{S_\odot}\right). \tag{44}$$

Now consider the position along x, y, and z axes in the coordinate system whose centered at the Sun, then the Sun's velocities with respect to this same group and referred to the same axes are given as ($X_\odot^\bullet = -\overline{V}_x$). ($Y_\odot^\bullet = -\overline{V}_y$), and ($Z_\odot^\bullet = -\overline{V}_z$). Therefore, we obtained the solar elements with radial velocities considered w.r.v.c. as follows:

$$S_\odot = \sqrt{(X_\odot^\bullet)^2 + (Y_\odot^\bullet)^2 + (Z_\odot^\bullet)^2}, \tag{45}$$

$$\alpha_A = \tan^{-1}\left(\frac{Y_\odot^\bullet}{X_\odot^\bullet}\right), \tag{46}$$

$$\delta_A = \tan^{-1}\left(\frac{Z_\odot^\bullet}{\sqrt{(X_\odot^\bullet)^2 + (Y_\odot^\bullet)^2}}\right), \tag{47}$$

where (l_A, α_A) is the Galactic, longitude and right ascension of the solar apex and (b_A, δ_A) are the Galactic, latitude and declination of the solar apex, where ($S_\odot$) is considered as the absolute value of Sun's velocity relative to our groups under investigations.

6. Conclusion

In this paper, we have investigated the poorly studied open clusters, Koposov 12 (FSR 802) and Koposov 43 (FSR 848), using PPMXL and Gaia DR2 data via cross-match. Here, we re-estimated the cluster center and core radius based on their RDP.

To derive their fundamental and kinematical parameters within (J, H, K_s, G, G_{BP}, and G_{RP}) regions, we have estimated their membership (utilizing proper motions and magnitude uncertainties) with probabilities $\geq 50\%$, and we have found 285 and 310 member stars, respectively.

Based on the NIR and Gaia (CMDs) of the cluster members, we have estimated the cluster parameters (reddening, distance modulus, and ages) listed in Table 6, which are in good agreement with previous studies. The dynamical and kinematical properties of these clusters (tidal radii, crossing, relaxation and evaporation times, space velocities, and VEPs) are numerically mentioned in Table 7.

Based on the estimated dynamical evolution parameter ($\tau \gg 1$), i.e., $\tau = 15.38 \pm 3.92$ for Koposov 12 (FSR 802) and 36.72 ± 6.06 for Koposov 43 (FRS 848), we infer that these clusters are dynamically relaxed.

Acknowledgements

The author is thankful to the referees for many useful comments and continuous encouragement, which highly improved the level of this paper. This work presents results from the European Space Agency space mission Gaia. Gaia data are being processed by the Gaia DPAC. Funding for the DPAC is provided by national institutions, in particular, the institutions participating in the Gaia Multilateral Agreement. The Gaia mission website is https://www.cosmos.esa.int/gaia. The Gaia archive website is https://archives.esac.esa.int/gaia. Also, it is worthy to mention that this publication made use of the data products from the PPMXL catalog. The author gratefully acknowledges the approval and the support of this research study by grant number SAR-2018-3-9-F-7591 from the Deanship of Scientific Research at Northern Border University, Arar, Saudi Arabia.

References

Adams F. C., Myers P. 2001, Astrophys. J., 533, 744
Binney J., Merrifield M. 1998, Galactic Astronomy, Princeton Series in Astrophysics, Princeton University Press
Binney J., Termaine S. 2008, Galactic Dynamics, 2nd edn. Princeton University Press, Princeton, NJ USA

Bisht D., Yadav R. K. S., Shashikiran G., *et al.* 2019, Mon. Not. R. Astron. Soc., 482, 1471B
Bisht D., Elsanhoury W. H., Zhu Q. 2020a, Astron. J., 160, 119B
Bisht D., Zhu Qingfeng, Yadav R. K. S. *et al.* 2020b, Mon. Not. R. Astron. Soc., 494, 607
Blaauw A., Schmidt M. 1965, Galactic Structure. University of Chicago Press, Chicago
Bland-Hawthorn J., Sharma S. *et al.* 2019, Mon. Not. R. Astron. Soc., 486, 1167
Bonatto C., Bica E., Girardi L. 2004, Astron. Astrophys., 415, 571
Bonatto C., Bica E. 2009, Mon. Not. R. Astron. Soc., 397, 1915
Bovy J. 2017, Mon. Not. R. Astron. Soc., 468, L63
Cantat-Gaudin T., Jordi C. *et al.* 2018, Astron. Astrophys., 618A, 93C
Cantat-Gaudin T., Anders F. 2020, Astron. Astrophys., 663A, 99C
Carpenter J. M. 2001, Astron. J., 121, 2851
Dib S., Schmeja S., Parker R. J. 2018, Mon. Not. R. Astron. Soc., 473, 849
Claria J. J., Lapasset E. 1986, Astron. J., 91, 326
Dutra C. M., Santiag B. X., Bica E. 2002, Astron. Astrophys., 381, 219
Elsanhoury W. H., Hamdy M. A., Nouh, M. I. *et al.* 2011, ISRN Astron. Astrophys., ID 127030
Elsanhoury W. H. 2015, Astrophysics, 58, 522
Elsanhoury W. H., Nouh M. I., Abdel-Rahman H. I. 2015 Rev. Mex. Astron. Astrofís., 51, 197
Elsanhoury W. H., Haroon A. A., Chupina N. V., *et al.* 2016, New Astron., 49, 32E
Elsanhoury W. H., Postnikova E. S., Chupina N. V. *et al.* 2018, Astrophys. Space Sci., 363, 58
Elsanhoury W. H., Nouh M. I. 2019, New Astron., 72, 19
Elsanhoury W. H. 2020, Bulg. Astron. J., 32, 83
Evans D. W. *et al.* 2018, Astron. Astrophys., 616, A4
Fich M., Tremaine S. 1991, Annual Rev. Astron. Astrophys. 29, 409
Fiorucci M., Munari U. 2003, Astron. Astrophys., 401, 781
Freedman D., Diaconis P. 1981, Z. Wahr. Geb., 57, 453
Froebrich D., Meusinger H., Scholz, A. 2008, Mon. Not. R. Astron. Soc., 390, 1598
Fukushige T., Heggie D. C. 2000, Mon. Not. R. Astron. Soc., 318, 753
Fürnkranz V., Meingast S., Alves J. 2019, Astron. Astrophys., 624, L11
Gaia Collaboration *et al.* 2018, Astron. Astrophys., 616A, 1G
Glushkova E. V., Koposov S. E., Zolotukhin I. Y. *et al.* 2010, Astron. Lett., 36, 75
Hendy Y. H. M. 2018, NRIAG J. Astron. Astrophys., 7, 180
Joshi Y. C., Maurya J., John, A. A. *et al.* 2020, Mon. Not. R. Astron. Soc., 492, 3602
Kharchenko N. V., Piskunov A. E., Schilbach E. *et al.* 2013, Astron. Astrophys., 558, A53
King I. 1962, Astron. J., 67, 471
Koposov S. E., Glushkova E. V., Zolotukhin I. Yu. 2008, Astron. Astrophys., 486, 771
Lada C. J., Lada E. A. 2003, Annu. Rev. Astron. Astrophs., 41, 57
Liu J.-C., Zhu Z., Hu B. 2011, Astron. Astrophys., 536, A102
Maciejewski G., Niedzielski A. 2007, Astron. Astrophys., 467, 1065
Maciejewski G., Mihov B., Georgiev T. 2009, Astron. Nach., 330, 851
Marigo P., Girardi L., Bressan A. *et al.* 2017. Astrophys. J., 835, 77
Mathieu R. D., Latham D. W. 1986, Astron. J., 92, 1364
Michalik D., Lindegren L., Hobbs D. 2015, Astron. Astrophys., 574, A115
Mihalas D., Binney J. 1981, Galactic Structure "Structure and Kinematics," 2nd edn. W. H. Freeman and Company, San Francisco
Monet D. G., Levine S. E., Canzian B. *et al.* 2003, Astron. J., 125, 984
Nilakshi S. R., Pandey A. K., Mohan V. 2002, Astron. Astrophys., 383, 153
Nouh M. I., Elsanhoury W. H. 2020, Astrophysics, 63, 179
Piatti A. E. 2016, Mon. Not. R. Astron. Soc., 463, 3476
Postnikova E. S., Elsanhoury W. H., Sariya D. P., *et al.* 2020, Res. Astron. Astrophys., 20, 16
Rangwal G., Yadav R. K. S., Durgapal A. *et al.* 2019, Mon. Not. R. Astron. Soc., 490, 1383
Roeser S., Demleitner M., Schilbach E. 2010, Astron. J., 139, 2440
Röser S., Schilbach E., Piskunov A. E. *et al.* 2011, Astron. Astrophys., 531, A92
Röser S., Elena S. 2019, Astron. Astrophys., 627A, 4R
Salpeter E. E. 1955, Astron. J., 121, 161
Sampedro L., Dias W. S., Alfaro E. J. *et al.* 2017, Mon. Not. R. Astron. Soc., 470, 3937
Sariya D. P., Jiang I.-G., Yadav R. K. S. 2018, IAU Symp. 330, Astrometry and Astrophysics in the Gaia Sky, ed. A. Recio-Blanco *et al.* Cambridge: Cambridge University Press, 251
Schlafly E. F., Finkbeiner D. P. 2011, Astron. J., 737, 103
Schlegel D. J., Finkbeiner D. P., Davis M. 1998, Astron. J., 500, 525
Skrutskie M. F. *et al.* 2006, Astron.J., 131, 1163
Smart W. M. 1968, Stellar Kinematics, Longmans, London
Soubiran C. *et al.* 2018, Astron. Astrophys., 619, A155
Tadross A. L. 2011, J. Korean Astron. Soc., 44, 1
Tadross A. L., Bendary R. 2014, J. Korean Astron. Soc., 47, 137
Taylor M. B. 2005, in Astronomical Data Analysis Software and Systems XIV, eds P. Shopbell M. Britton, R. Ebert, ASP Conference Series, 347, 29
van Rhijn P. J. 1965, Pub. Kapteyn Astron. Lab. Groningen, No. 47
Weiler M. 2018, Astron. Astrophys., 617, A138
Wilking B. A., Lada C. J. 1983, Astrophys. J., 274, 716
Yadav R. K. S., Glushkhova E. V., Sariya D. P. *et al.* 2011, Mon. Not. R. Astron. Soc., 414, 652
Zeidler P., Nota A., Grebel E. K. *et al.* 2017, Astron. J., 153, 122